X-ray absorption spectra for transition metal high-κ dielectrics: Final state differences for intra- and inter-atomic transitions

G. Lucovsky[a)]
Departments of Physics, Materials Science and Engineering, and Electrical and Computer Engineering, North Carolina State University, Raleigh, North Carolina 27695-8202

J. G. Hong and C. C. Fulton
Materials Science and Engineering, North Carolina State University, Raleigh, North Carolina 27695-8202

Y. Zou, R. J. Nemanich, and H. Ade
Department of Physics, North Carolina State University, Raleigh, North Carolina 27695-8202

(Received 31 March 2004; accepted 26 April 2004; published 19 August 2004; published 19 August 2004)

This article applies x-ray absorption spectroscopy to a study of the electronic structure of the high-k gate dielectrics, TiO_2, ZrO_2, and HfO_2. Qualitative and quantitative differences are identified between *intra-atomic* transitions such as the Zr $3p$-state, $M_{2,3}$ core state absorptions which terminate in TM $4d^*$- and $5s^*$-states, and *inter-atomic* transitions such as the Zr $1s$- and O $1s$-state K_1 absorptions which terminate in Zr $4d^*$- and $5s^*$-states that are mixed with O atom $2p^*$ states through nearest neighbor bonding interactions. Differences between the spectral peak energies of the lowest d^*-features in the O K_1 spectra are demonstrated to scale with optical band gap differences for TiO_2, ZrO_2, and HfO_2, providing important information relevant to applications of TM oxides as high-κ gate dielectrics in advanced Si devices. This is demonstrated through additional scaling relationships between (i) conduction band offset energies between Si and the respective dielectrics, and the optical band gaps, and (ii) the conduction band offset energies, and the electron tunneling masses as well. © *2004 American Vacuum Society.* [DOI: 10.1116/1.1771670]

I. INTRODUCTION

There has been considerable interest in transition metal (TM) and lanthanide series rare earth (RE) atom oxides, and their silicate and aluminate alloys as *replacement or alternative* high-κ dielectrics for SiO_2 in advanced silicon field effect transistors (FETs) requiring a gate oxide dielectric capacitance per unit area, C_{ox}, greater than $4\times10^{-6}\,\mathrm{F\,cm^{-2}}$.[1–3] These levels of capacitance, although attainable in thermally-grown SiO_2, cannot be utilized in devices because the physical SiO_2 thickness required is less than 1.0 nm, and this leads to excessively high tunneling leakage currents, $>100\,\mathrm{A\,cm^{-2}}$ at a 1 V oxide bias. Tunneling leakage at these levels degrades FET performance and reduces reliability as for example the time to dielectric breakdown (TDDB) under accelerated high-field bias.

High-k dielectrics can achieve these increased levels of capacitance per unit area, but at a physical film thickness which is increased by the ratio of their respective dielectric constants, k_a, to that of SiO_2, ~3.9. Since k_a ranges from 20 to more 60 for the group IVB (Ti, Zr, and Hf), group IIIB (Sc, Y, and La) TM oxides, as well as for the trivalent lanthanide RE oxides, the thickness increases of at least fivefold are sufficient to predict reductions of the tunneling current by many orders of magnitude. However, the tunneling leakage also depends on the square root of the product of (i) the height of the barrier or conduction band offset energy between the conduction band of Si, and the lowest conduction band states of the dielectric, E_B, and (ii) the effective mass of the tunneling electrons, m^*_{eff}.[4] This study includes spectroscopic results that demonstrate that the band gaps of the TM and RE oxides, as well as their respective silicate and aluminate alloys, are significantly reduced with respect to the band gap of SiO_2. Scaling arguments are used to demonstrate that these band gap reductions are accompanied reductions in E_B, as well as in m^*_{eff}. The band gap, E_B and m^*_{eff}, reductions scale with the atomic d-state energies of TM and RE atoms, and provide important insights for the identification of the particular TM and RE oxides, silicates, and aluminates that have the potential to meet international industry roadmap targets for device performance with respect to gate leakage currents.[1–3]

The transition from thermally-grown SiO_2 gate dielectrics to deposited high-κ gate dielectrics is also wrought with many technological difficulties relative to film deposition and process integration.[1–6] This article does not address these technology issues, but instead focuses on fundamental differences in the electronic structure between the group IVB TM oxides and SiO_2. The most significant differences are manifested in the character of the electronic states that comprise the lowest conduction bands. These are spatially localized d^*-states in the TM and RE dielectrics, in marked contrast to the extended s^*-states that comprise the lowest conduction band in SiO_2. As noted above, the energies of the lowest energy d^*-state bands relative to the top of the conduction band in crystalline Si define the conduction band offset energy barrier, E_B, for electron injection into the dielectric, as well as for electron tunneling through the dielectric. These offset energies have emerged as a critical consid-

a)Electronic mail: lucovsky@unity.ncsu.edu

eration for meeting roadmap targets for attainment of high capacitance, $>4\times10^{-6}\,\mathrm{F\,cm^{-2}}$, with low direct tunneling, or more generally leakage currents in alternative gate dielectrics in aggressively scaled devices.[1–3]

This article uses x-ray absorption spectroscopy (XAS) to study the electronic structure of the high-K gate dielectrics, TiO_2, ZrO_2, and HfO_2. Qualitative and quantitative differences are identified between *intra-atomic* transitions such as the Zr $3p$-state, $M_{2,3}$ core state absorptions which terminate in TM $4d^*$- and $5s^*$-states, and *interatomic* transitions such as the Zr $1s$- and O $1s$-state K_1 absorptions which terminate in Zr $4d^*$- and $5s^*$-states that are mixed with O atom $2p^*$ states through nearest neighbor bonding interactions. Most importantly, differences between the spectral peak energies of the lowest d^*-features in the O K_1 absorption spectra of the TM oxides correlate linearly with reported optical band gap, E_g, differences for TiO_2, ZrO_2, and HfO_2, and thereby provide important information relevant to applications in advanced Si devices. In particular, the conduction band offset energies, E_B, between Si and high-k dielectrics scale approximately linearly with optical band gaps, E_g, and additionally the tunneling masses of the electrons, m^*_{eff}, scale with E_B, and therefore with E_g as well.[7]

II. EXPERIMENTAL STUDIES OF ELECTRONIC STRUCTURE

A. Experimental methods

The XAS studies were performed at the National Synchrotron Light Source (NSLS) at the Brookhaven National Laboratory (BNL) using total photoelectron yield to determine relative absorption strength of the spectral features. Thin film samples of ZrO_2 and HfO_2, approximately 30 nm thick, were prepared by remote plasma assisted chemical vapor deposition (RPECVD).[8] Postdeposition annealing of deposited thin films was performed for 30 s to 1 min at 900 °C in an inert ambient, Ar.

TiO_2 thin films of approximately the same thickness were prepared by physical deposition of Ti, followed by *in situ* plasma-assisted oxidation at 300 °C; deposited films were then annealed in vacuum at 600 °C.[9] Characterization by high resolution transmission electron microscopy (HRTEM) imaging indicated that the TM oxide thin films of this study were crystalline in character, with the crystallite sizes in the nanoregime from ~3 to 20 nm.[10] HfO_2-TiO_2 oxide films were also deposited in the same manner, and provide an additional source of Ti $L_{2,3}$ spectra. Figure 2 contains Ti $L_{2,3}$ edge spectra for TiO_2 and a Ti-rich HfO_2-TiO_2 alloy with a ratio of 1.2.

B. Experimental approach

Figure 1 presents a schematic representation of the XAS transitions that are being addressed. For ZrO_2, these include the Zr K_1 and $M_{2,3}$ edges, and the O K_1 edge as well. These studies also include the Ti $L_{2,3}$ and Hf $N_{2,3}$ spectra, as well as the respective O K_1 edges for TiO_2 and HfO_2.

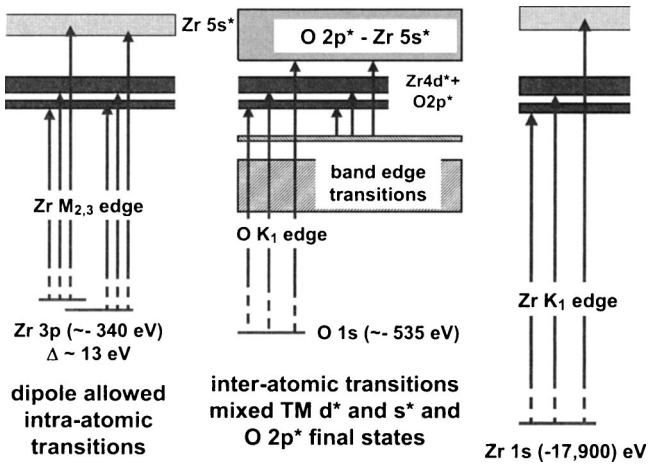

FIG. 1. Schematic representation of the intra-atomic Zr $M_{2,3}$, and inter-atomic atomic Zr K_1, O K_1 and band edge transitions for ZrO_2. The ordering of the energy states is derived from *ab initio* molecular orbital calculations on small neutral clusters (Refs. 5 and 11).

The schematic energy level diagrams of Fig. 1 include the (i) $\Delta(d^*_{1,2})$ splittings, and the $\Delta(d^*_1,s^*)$ energy difference between the lower energy d^*-state, and the lowest energy feature of the s^*-state band, These differences are used to quantify comparisons between: (i) *intra-atomic, dipole-allowed transitions* in which electrons are excited from relatively deep core states of the Ti, Zr or Hf atoms into empty states localized on the same atoms, and (ii) *interatomic* transitions in which electrons are excited either from TM or O atomic $1s$ core states into final states have a mixed O atom—TM atom character, and therefore are not restricted by atomic dipole selection rules.[5,11,12]

C. Intra-atomic, dipole allowed transitions

Figures 2(a), 2(b), and 2(c) are the Ti $L_{2,3}$, Zr $M_{2,3}$, and Hf $N_{2,3}$ spectra for the Ti-rich HfO_2-TiO_2 alloy with a ratio of 1.2, followed by ZrO_2, and HfO_2, respectively (see Table I). The features in each of these spectra are replicated for the respective spin–orbit split initial p-states, $np_{1/2}$ and $np_{3/2}$, where $n=2$ for TiO_2, 3 for ZrO_2, and 4 for HfO_2 are the principle quantum numbers of the respective L, M, and N shells.[12] For each of the spin–orbit split initial p-states, there are transitions to a d^*-state doublet, $3d^*$ for Ti, $4d^*$ for Zr, and $5d^*$ for Hf, and to a $4s^*$-, $5s^*$- or $6s^*$-state that is at a higher energy. Table I includes the positions of the spectral features for the Ti $L_{2,3}$ and Zr $M_{2,3}$ doublet components that are spectroscopically resolved, and the d^*-state energy of the spectral peak of Hf $N_{2,3}$ spectra, where the doublet components are not resolved. The energies of the Ti and Zr d^*-states and s^*-states have been obtained from fitting the features in the respective spectra by standard techniques using Gaussian line shapes with Lorentzian tails. The energies of the respective d^*-states obtained in this way are approximately the same as the positions of the spectral peaks in the spectra shown in Figs. 2(a) and 2(b). The spectral peaks of the s^*-state features are broader, and there is also spectral overlap with d^*-states, so that the fitting procedure is the

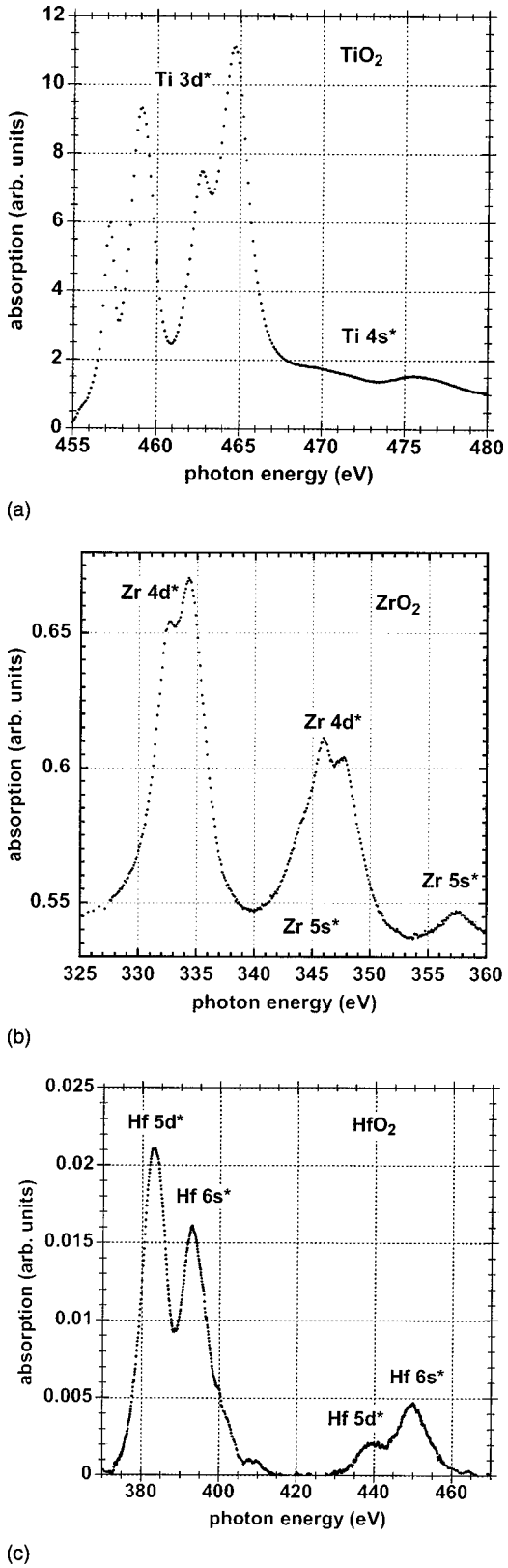

FIG. 2. (a) Ti $L_{2,3}$, (b) Zr $M_{2,3}$, and (c) Hf$N_{2,3}$ x-ray absorption spectra.

most reliable way to obtain these energies. The L_2, M_2, and N_2 features are shifted in energy with respect to the corresponding L_3, M_3, and N_3 features by the spin–orbit splittings of the respective $2p$-, $3p$-, and $4p$-initial states. The spectroscopic splittings of 5.6 eV±0.3 eV for Ti, 13.3 eV for Zr, and for 57.6 eV±0.3 eV for Hf are in excellent agreement with X-*ray Data Handbook Values*.[13]

TABLE I. Summary of experimental results for d^* and s^* features in XAS spectra of Figs. 2(a), 2(b), and 2(c), 4(a), 4(b), and 4(c), and 5.

	Energy (±0.2 eV)			Energy (±0.3 eV)	
Spectrum	d_1^*	d_2^*	s^*	$\Delta(d_{1,2}^*)$	$\Delta(d_1^*, s^*)$
Ti K_1[a]	4960	4962.5	4968.6	2.5	8.6
Ti L_2	462.7	464.7	475.3	2.0	10.0
Ti L_3	457.2	459.1	469.7	1.9	9.8
O K_1(Ti)	530.1	532.8	539.5	2.7	8.4
Zr K_1	18008[b]	18008[b]	17998	3[c]	13[d]
Zr M_2	345.9	347.7	357.5	2.2	11.7
Zr M_3	332.6	334.8	344.5	2.2	11.9
O K_1(Zr)	532.2	535.4	542.3	3.2	10.1
Hf N_3	382.7[b]	382.7[b]	392.7	<3.5[c]	10[d]
O K_1(Hf)	532.5	536.8	541.5	4.3	9.0

[a]References 16 and 17.
[b]Not resolved.
[c]Estimated from linewidth.
[d]Average separation.

The relative absorption strengths for the d^* and s^* features in the spectra for TiO_2, ZrO_2, and HfO_2 are markedly different. The s^*-state spectral features are very weak in the TiO_2 L_3 and L_2 spectra, the corresponding absorptions strengths increase modestly for the ZrO_2 M_3 and M_2 spectra, and then are significantly stronger for the HfO_2 N_3 and N_2 spectra. These relative intensities are in qualitative agreement with relative intensities based on hydrogenic Rydberg states.[14]

Figures 3(a) and 3(b) are $L_{2,3}$ spectra of TiO_2. Figure 3(a) shows the same *double doublet* structure of the Ti-rich HfO_2–TiO_2 alloy spectrum in Fig. 2(a); however, due to the rutile crystalline structure, there is a splitting of the lower energy L_3 doublet component. The two- and threefold degeneracies of L_3 components are completely removed. The doubly degenerate feature at ~459 eV is split into two peaks with a separation of ~1.6 eV. The triply degenerate feature at ~457.2 eV is split into three features at 455.7 eV, 456.4 eV, and 457.3 eV.

D. Inter-atomic O and K_1 edge, and band edge transitions

Figures 4(a), 4(b), and 4(c) are O K_1 edge spectra, respectively for TiO_2, ZrO_2, and HfO_2. Each of these spectra is qualitatively similar, displaying a well-resolved d^*-doublet at the absorption threshold, and a broader s^*-feature with some additional structure at higher energies that may be due to transitions to p^*-states. The positions of the spectral features, and the $\Delta(d_{1,2}^*)$ and respective $\Delta(d_1^*, s^*)$ spectroscopic splittings determined from the peaks in Figs. 4(a), 4(b), and 4(c) are included in Table I. The $\Delta(d_{1,2}^*)$ splitting increases in going from TiO_2 to ZrO_2, and then to HfO_2, by ~0.5 eV and 0.8 eV, respectively. The spectral overlap between the higher energy d^*-state, d_2, and the lowest energy s^*-feature decreases from TiO_2 and ZrO_2 to HfO_2. Contri-

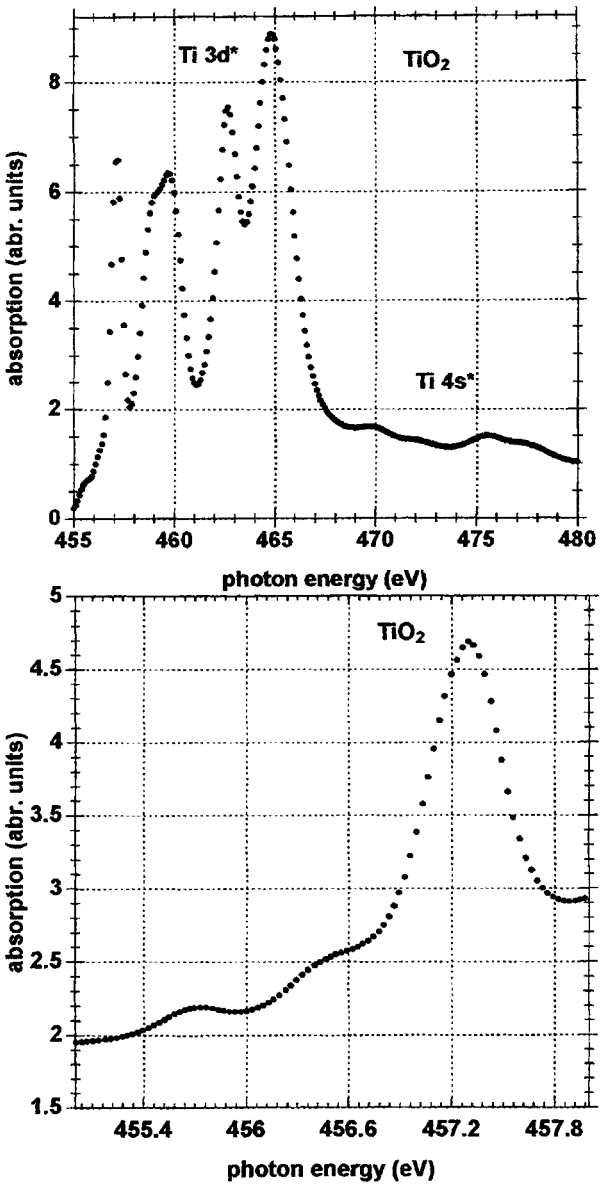

FIG. 3. (a) Ti $L_{2,3}$ spectra for TiO_2. (b) Near edge structure on Ti L_3 feature.

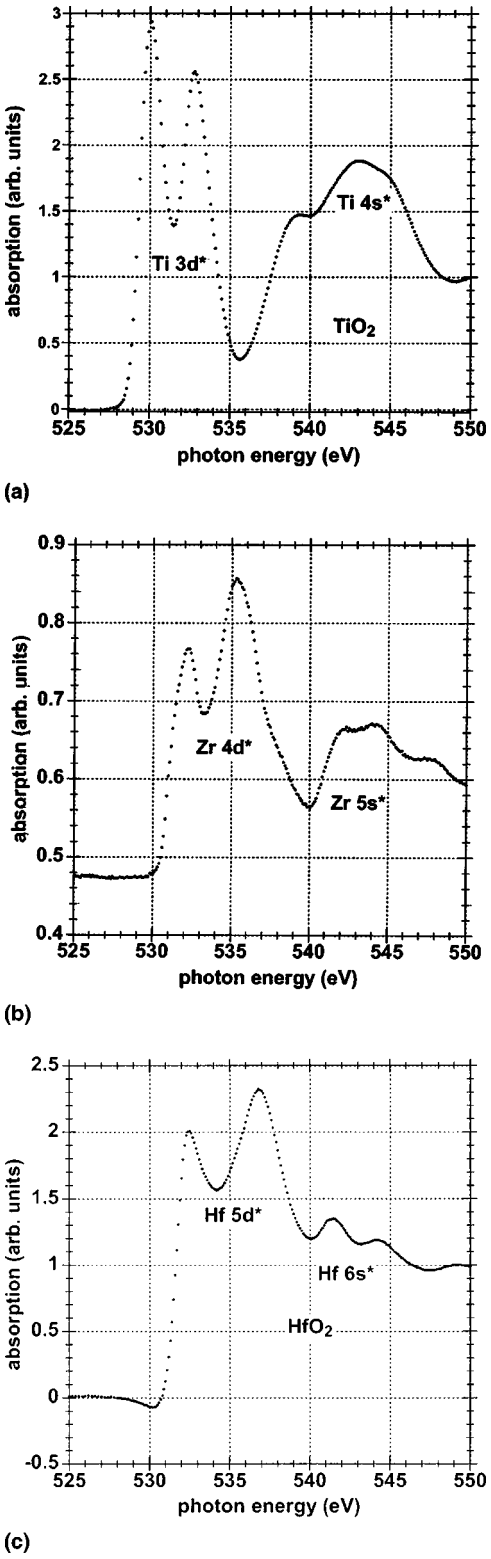

FIG. 4. O K_1 spectra for (a) TiO_2, (b) ZrO_2, and (c) HfO_2.

butions to the spectral overlap include (i) increases in the respective $\Delta(d_1^*,s^*)$ splittings from TiO_2 (2.7 eV) to ZrO_2 (3.2 eV) to HfO_2 (4.3 eV), (ii) decreases in $\Delta(d_2^*,s^*)$ energy separations (not included in Table I) of approximately 6.7 eV of 6.9 eV, respectively, for TiO_2 and ZrO_2, to 5.0 eV for HfO_2, and finally, (iii) increases in the spectral half-width of the d_2^* features that scale monotonically with the atomic number of the TM atom.

The Zr K_1 spectrum for ZrO_2 is shown in Fig. 5. This spectrum is similar to those presented in Ref. 15, where markers indicate that the positions of features assigned to $4d^*$- and $5s^*$-states. The energies of the features are essentially the same for all of the crystalline phases of ZrO_2. Since transitions from the Zr $1s$-state to Zr $4d^*$- and $5s^*$-states are not dipole-allowed, the Zr K_1 edge spectrum is qualitatively similar to the O K_1 edge spectrum in which the final states also involve a mixing between Zr $4d^*$- and $5s^*$-states, and O $2p^*$-states. This is reflected in the values of $\Delta(d_{1,2}^*)$ and $\Delta(d_1^*,s^*)$ presented in Table I. The doublet $4d^*$-features are not spectroscopically resolved in Fig. 5, or in the spectra in Ref. 15, as it is in the O K_1 spectrum in Fig. 4(b).

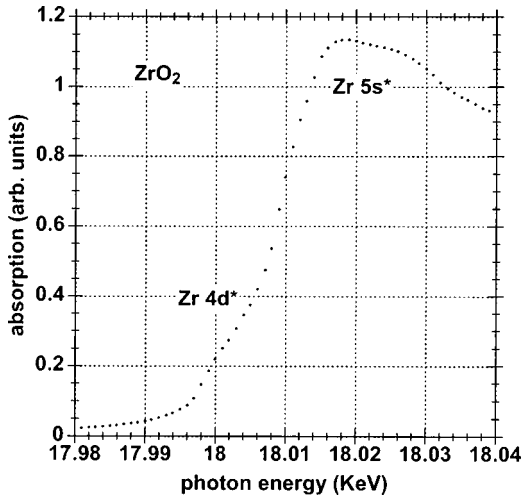

FIG. 5. Zr K_1 XAS spectrum.

Ti K_1 and Hf K_1 edge spectra have not been obtained for the thin film samples prepared for this study. However, there have been several published studies of the Ti K_1 edge in the rutile and anatase crystal forms of TiO_2.[16,17] Published results for the Ti K_1 edge of TiO_2 in the rutile phase are included in Table I.[16,17] A comparison indicates a similar *x*-axis (energy) behavior between the O K_1 spectra for the nanocrystalline TiO_2 film of this study, and the published rutuile Ti K_1 spectrum.[16,17] The *d*-state splittings are the same to within experimental error; 2.5 ± 0.3 eV for the Ti K_1 spectrum, and 2.7 ± 0.3 eV for the O K_1 spectrum. In addition, the average difference in energy between the d_1^*-state feature, and the first s^*-state spectral peak are the same to within the experimental error of ±0.3 eV: 8.6 ± 0.3 eV for the Ti K_1 spectrum, and 8.4 ± 0.3 eV for the O K_1 spectrum. However, as in the case of ZrO_2, the relative intensities of the d^*- and s^*-features are different in the Ti K_1 and O K_1 spectra.

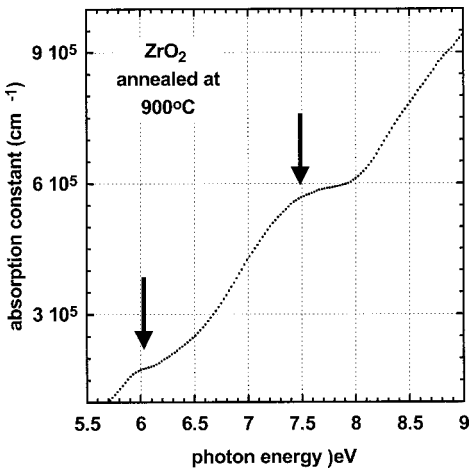

FIG. 6. Absorption edge spectrum for ZrO_2 annealed at 900 °C. The arrows indicate the band edge $4d^*$ features.

E. Optical absorption edge spectrum

Figure 6 contains a plot of the optical absorption constant, α, versus photon energy for ZrO_2, as obtained from an analysis of vacuum ultraviolet spectroscopic ellipsometry data.[18] The band edge, or threshold for optical absorption is at ~5.7 eV, essentially the same as reported from complementary measurements of the photoconductivity.[19] The relative intensities of the d^*-state absorption between 5.7 and 6 eV and the s^*-state absorption at higher photon energies is similar to the relative intensities of the corresponding features in the Zr K_1 spectrum, but the energy scales are markedly different. For the Zr K_1 spectrum, the initial state is the Zr $1s$-state at -18 keV, and for the band edge transitions, the initial states are O $2p\ \pi$ nonbonding states at the top of the valence band.

III. DISCUSSION

A. Spectroscopic results

This section distinguishes between the intra-atom Ti $L_{2,3}$, Zr $M_{2,3}$, and Hf $N_{2,3}$ edge spectra of Figs. 2(a), 2(b), and 2(c), and the interatomic (i) Ti O K_1, Zr O K_1, and Hf O K_1 spectra of Figs. 4(a), 4(b), and 4(c), (ii) Zr K_1 edge spectra of Fig. 5, and (iii) band edge ZrO_2 spectra of Fig. 6.

Figure 1 indicates the intra-atomic transitions that contribute to the six-distinct features the Zr $M_{2,3}$ spectrum of Fig. 2(b). This schematic representation has been applied to the Ti $L_{2,3}$ Hf $N_{2,3}$ spectra as well, and also applies to the corresponding group IIIB TM (Sc, Y, and La) and the trivalent lanthanide RE atom oxide spectra. The spectral features are associated with transitions from relatively deep spin–orbit split Ti $2p$-, Zr $3p$-, and Hf $4p$-states, typically 200–500 eV below vacuum, to empty 3, 4, or $5d^*$- and 4, 5, or $6s^*$-states, respectively. These transitions are atomiclike in character and are significantly not-changed by second neighbors as has been shown for the Zr $M_{2,3}$ spectra through the comparisons that include Zr homogeneous, as well as chemically phase-separated silicate alloys.[12] The relative intensities of final d^*-states in the Ti and Zr spectra are consistent with the lower energy pair in each spectral component being the $d_{3/2}$ state with a spectral weighting of 4, and the higher energy component being the $d_{5/2}$ state with a spectral weighting of 6. Since the local symmetries of the Ti and Zr atoms are effectively sixfold coordinated in TiO_2 and eightfold coordinated in ZrO_2, and since the ordering of the d^*-states in the respective spectra are the same, this demonstrates that the d^*-state spitting is not determined by local symmetry. A splitting associated with the local symmetry would have yielded the reverse ordering of the doubly and triply degenerate d^*-states for *sixfold* coordinated TiO_2 and approximately *eightfold* coordinated ZrO_2.[11]

The O K_1 edge spectra for TiO_2 in Fig. 4(a), ZrO_2 in Fig. 4(b), and HfO_2 in Fig. 4(c) are assigned to transitions from the O $1s$-state to final *bandlike* states that have a mixed (i) O $2p^*$-state, and (ii) TM 3, 4, or 5 d^*- and TM 4, 5 or 6-s^*-state character, respectively. In contrast to the order of magnitude intensity variation between the respective, (i) Ti

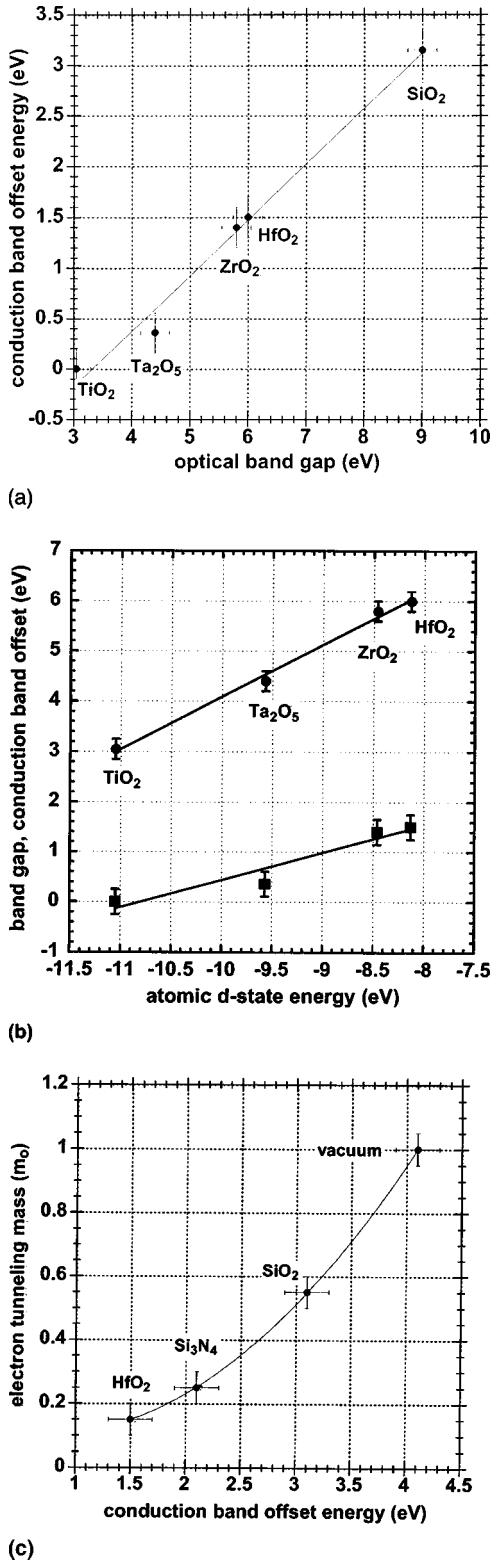

FIG. 7. (a) Conduction band offset energy, E_B, vs optical band gap, E_g, for representative TM oxides, and SiO_2. The E_g values, as well as the E_B values for the TM oxides are from Ref. 7. The E_g value for SiO_2 is also from Ref. 7; however, the E_B value is the accepted experimental value, 3.15 eV, and is about 0.35 eV less than the calculated value of Ref. 2. (b) E_B and E_g for the TM oxides of (a), as functions of the TM atom *d*-states in the $n+1\,s^2$, $n\,d^{\gamma-2}$ configurations, where $\gamma=4$ and 5, for the respective group IVB and VB oxides (Ref. 28). (c) m_{eff} versus E_B for representative gate dielectrics. The solid line is a quadratic fit to the points.

and Zr, and (ii) Hf d^*- and s^*-spectral features in Figs. 2(a) and 2(b), and Fig. 2(c), the *corresponding* d^*- and s^*-related features in Figs. 4(a), 4(b), and 4(c), have relative intensities that differ by no more than a factor of 2. This demonstrates that the matrix elements for absorption to the d^*- and s^*-state features in the respective O K_1 spectra are not determined by the Rydberg-type transition probabilities, but are related to the mixed nature of the final states.[14]

The Zr K_1 edge spectra in Fig. 5, and the Ti and Zr K_1 spectra discussed at length in Refs. 15, 16, and 17, are also inter-atomic spectra. The transitions between the Zr and Ti 1*s*-states to the respective Zr 4d^*- and 5s^*-states, and Ti 3d^*- and 4s^*-states are not dipole-allowed, and the lowest energy transitions are to final states with a mixed O 2p^*-state, and Ti or Zr d^*- and s^*-state character. This interpretation of the Zr and Ti K_1 spectra is supported by the fact that these transitions have features at higher energy that are used in extended x-ray absorption fine structure (EXAFS) studies to determine nearest neighbor Zr and O, and Ti and O bond lengths, and second and more distant neighbor interatomic separations.[20]

Even though the final states have similar atomic character, the relative absorptions of the 4d^* and 5s^* features in the O K_1 and Zr K_1 spectra of ZrO_2 are markedly different, and therefore reflect differences in the respective O 1*s*- and Zr 1*s*-ground state wave functions, and their effect on the transition probabilities for these absorptions. This comparison also holds for the relative absorptions of the 3d^* and 5s^* features in the O K_1 and Ti K_1 spectra of TiO_2.

The relative absorption strengths for the 4d^* and 5s^* features in the Zr K_1 spectrum in Fig. 4 bear some resemblance to features assigned to the same states in the band edge absorption spectrum in Fig. 6. For example, the threshold d^*-state feature has a markedly lower absorption constant than other d^*- and s^*-states features at higher energies. This is the case even though the initial states are very different; the localized Zr 1*s*-core state for the Zr K_1 spectrum, and the more delocalized O 2*p* nonbonding π states for the band edge absorptions.

Finally, and perhaps most important, a comparison between the energies of the first spectral peak of the respective O K_1 spectra, 530.1 eV for TiO_2, 532.4 eV for ZrO_2, and 532.6 for HfO_2, indicates that the differences between these energies are equal, to within an experimental uncertainty of ± 0.3 eV, to the respective differences in reported *nominal band gap energies* of 3.1 eV for rutile TiO_2,[11] 5.6 eV for ZrO_2,[19] and 5.8 eV for HfO_2.[19] This comparison carries over as well to high-*k* complex oxide such as $GdScO_3$ and $DyScO_3$.[21]

B. Conduction band offset energies and tunneling

In order to reduce direct tunneling in FETs with EOT$<$1.5 nm, and extending below 1 nm, there has been a search for alternative dielectrics with significantly increased dielectric constants, *k*, with respect to SiO_2. This allows increases in physical thickness proportional to *k* for a given gate dielectric capacitance, thereby having the potential to significantly

reduce direct tunneling. However, *increases* in k are generally accompanied by *decreases* in the optical band gap, E_g, the conduction band offset energy with respect to Si, E_B, and the effective electron tunneling mass, m^*_{eff}. These tradeoffs are quantified by the introduction of a tunnelling figure of merit, Φ_m, given by

$$\Phi_m = k[E_B \cdot m^*_{\text{eff}}]^{0.5}. \quad (1)$$

Robertson and co-workers have developed a model for obtaining band gaps and conduction band offset energies for representative gate dielectric materials including SiO_2 and Ta_2O_5 as well as the high-k dielectrics of this article.[7,23] Figure 7(a) is plot of E_B vs E_g in which the experimentally determined band offset energy for SiO_2, 3.15 eV used instead of the calculated values from Ref. 2. The relationship is approximately linear, as indicated by the fit to the points in Fig. 7(a). Figure 7(b) contains plots of E_g and E_B as a function of the atomic d-state energy of the TM atoms for the TM oxides of Fig. 7(a). This new scaling law follows from the spectroscopic studies of this article, and the *ab initio* calculations that are in process.[24] As noted above, O K_1 spectra of TM oxides provide quantitative information about relative band gaps for TM oxides, and for the extension of this relationship to more complex oxide alloys and compounds as well. For example, combined with Auger electron spectroscopy and x-ray photoelectron spectroscopy studies, XAS spectra have provide important information relative to the compositional dependence of conduction band energies in Zr and Hf silicate alloys. Based on these comparisons, several of the group IVB and VB TM oxides with the highest dielectric constants, e.g., TiO_2, and Nb_2O_3 and Ta_2O_3, have offset energies below 1 eV that correlate with either high tunneling leakage, and or electric field assisted injection into low-lying conduction band traps associated with these atoms.[25] Based on scaling with atomic d-states, (i) the group IVB oxides of Zr and Hf and their respective silicate, and aluminate alloys, as wells as (ii) the group IIIB, and lanthanide RE series oxides, and their respective silicate and aluminate alloys are expected to have conduction band offset energies greater than about 1.2–1.3 eV, and therefore, have the potential for meeting roadmap targets for tunneling leakage current,[3] provided the electron tunneling mass, m_{eff}, does not decrease significantly with decreasing E_B.

Figure 7(c) is a plot of the electron tunneling mass, m_{eff} vs the conduction band offset energy, E_B. The linear portion of this plot for E_B between about 2.5 and 4.1 eV is in accord with the Franz two-band model of Refs. 26 and 27, and applies when the conduction band states are free electronlike with predominantly s^*-character. The projected values for m_{eff} when E_B less than about 2 eV are attributed to a change in the character of the lowest conduction band states, from s^*-extended states in SiO_2 and Si_3N_4, to significantly more localized d^*-states in the TM and RE dielectrics. Based on an analytic continuation of the quadratic fit in Fig. 7(c), a 1.2–1.3 eV offset energy is expected to be a good lower limit for dielectrics that will meet roadmap targets for aggressive scaling of EOT down to at least 1.0 nm.[1–4,22]

ACKNOWLEDGMENTS

This research is supported in part by the Office of Naval Research, the Semiconductor Research Corporation, and the Semiconductor Research Corporation/International Sematech Front End Processes Center.

[1]G. D. Wilk, R. W. Wallace, and J. M. Anthony, J. Appl. Phys. **87**, 484 (2000).
[2]G. D. Wilk, R. W. Wallace, and J. M. Anthony, J. Appl. Phys. **89**, 5243 (2001).
[3]*International Technology Roadmap for Semiconductors* (2001 ed.) at http://public.itrs.net.
[4]C. L. Hinkle and G. Lucovsky, Microelectron. Eng. **72**, 257 (2004).
[5]G. Lucovsky, G. B. Rayner, Y. Zhang, G. Appel, and J. L. Whitten, Appl. Surf. Sci. **216**, 215 (2003).
[6]E. W. A. Young and V. Kauschik, in *High-k Gate Dielectrics*, edited by M. Houssa (Institute of Physics, Bristol, 2003), p. 449.
[7]J. Robertson, J. Vac. Sci. Technol. B **18**, 1785 (2000).
[8]G. B. Rayner, Jr., D. Kang, Y. Zhang, and G. Lucovsky, J. Vac. Sci. Technol. B **20**, 1748 (2002).
[9]C. C. Fulton, G. Lucovsky, and R. J. Nemanich, Appl. Phys. Lett. **84**, 580 (2004).
[10]G. B. Rayner, D. Kang, and G. Lucovsky, J. Vac. Sci. Technol. B **21**, 1783 (2003).
[11]P. A. Cox, *Transition Metal Oxides* (Oxford Science Publications, Oxford, 1992), Chap. 2.
[12]G. Lucovsky, G. B. Rayner, Jr., D. Kang, G. Appel, R. S. Johnson, Y. Zhang, D. E. Sayers, H. Ade, and J. L. Whitten, Appl. Phys. Lett. **79**, 1775 (2001).
[13]X-*ray Data Handbook*, edited by A. Thompson *et al.* (Lawrence Berkeley National Laboratory, University of California, Berkeley, CA, 2001).
[14]E. U. Condon and G. H. Shortly, *The Theory of Atomic Spectra* (Cambridge University Press, Cambridge, 1957), Chap. V.
[15]P. Lim, I.-W. Chen, and J. E. Penner-Han, Phys. Rev. B **48**, 10063 (1993-II).
[16]L. A. Grunes, R. D. Leapman, C. N. Nilker, R. Hoffman, and A. B. Kunz, Phys. Rev. B **25**, 7157 (1983).
[17]L. A. Grunes, Phys. Rev. B **27**, 2111 (1983).
[18]N. A. Stoute, D. E. Aspnes, and G. Lucovsky (unpublished).
[19]V. V. Afanas'ev and A. Stesmans, in *High-k Gate Dielectrics*, edited by M. Houssa (Institute of Physics, Bristol, 2003), p. 217.
[20]X-*Ray Absorption: Principles, Applications, Techniques of EXAFS, SEXAFS, and XANES*, edited by D. C. Koningsberger and R. Prins (Wiley, New York, 1988).
[21]G. Lucovsky and D. G. Schlom (unpublished).
[22]G. Lucovsky, Microelectron. Reliab. **43**, 1417 (2003).
[23]J. Robertson and C. W. Chen, Appl. Phys. Lett. **74**, 1164 (1999).
[24]Y. Zhang, G. Lucovsky, and J. L. Whitten (unpublished).
[25]R. S. Johnson, J. G. Hung, and G. Lucovsky, J. Vac. Sci. Technol. B **19**, 1606 (2001); **20**, 1126 (2002).
[26]W. Franz, in *Handbuch der Physik*, edited by S. Flugge (Springer, Berlin, 1965), Vol. XVIII, p. 155.
[27]J. Maserjian, J. Vac. Sci. Technol. **11**, 996 (1974).
[28]W. A. Harrision, *Elementary Electronic Structure* (World Scientific, Singapore, 1999), The Solid State Table.